

专任教师岗位低职高聘聘任申请表

姓 名	陶惠敏	出生年月	1992 年 6 月	参加工作时间	2021 年 4 月
现所在单位	机械学院	最高学历/学位	博士/博士	现聘专业技术职务	助教
现校聘岗位	专业技术九级	取得学历/学位时间	2021 年 1 月	聘任专业技术职务时间	2021 年 4 月
现省聘岗级	<input checked="" type="checkbox"/> 专业技术岗 <u>IX</u> 级 <input type="checkbox"/> 管理岗 _____ 级				
拟申请岗位	机械学院专任教师副高级 VII 级		校聘岗位类别	教学科研并重型	
是否按照专技身份享受校内绩效政策（双肩挑人员填写）			<input type="checkbox"/> 是 <input type="checkbox"/> 否		
任现职（岗级）以来取得业绩	A 类项目：__ 项				
	B 类项目： <u>1</u> 项	SCI 论文 1 篇			
	C 类项目：__ 项				
	业绩换算分值		4		
本人承诺	<p>本人知悉《第四轮岗位聘用实施办法》、《校内绩效工资实施方案》、《浙江水利水电学院“三定”方案（2020 版）》、《第四轮岗位聘任工作实施方案》等文件规定和各单位（部门）岗位聘任实施方案、岗位说明书，经慎重考虑申请相应岗位。承诺：</p> <p>1、以上所填内容全部属实，如有问题本人愿意承担一切责任；</p> <p>2、受聘岗位期间，能够履行相关文件要求及岗位说明书规定的岗位职责。</p> <p style="text-align: right;">本人签名： <u>陶惠敏</u></p> <p style="text-align: right;">2021 年 4 月 21 日</p>				
以上部分由申请人填写，应聘部门审核。以下由单位（部门）和管理服务岗位聘用委员会填写。					
原单位（部门）意见	<div style="display: flex; justify-content: space-between; align-items: center;"> <div> <input type="checkbox"/> 同意 <input type="checkbox"/> 不同意 </div> <div style="text-align: right;"> （部门盖章） ____ 年 ____ 月 ____ 日 </div> </div>				

<p>应聘单位（部门）聘任意见</p>	<p>1、经审核，申请人所填内容：<input type="checkbox"/>属实 <input type="checkbox"/>不属实</p> <p>2、是否符合所申请岗位的申报条件：<input type="checkbox"/>符合 <input type="checkbox"/>不符合</p> <p>3、是否同意聘任所申请岗位：<input type="checkbox"/>同意 <input type="checkbox"/>不同意</p> <p style="text-align: right;">（部门盖章）</p> <p style="text-align: right;">____年____月____日</p>
<p>专任教师岗位聘用委员会意见</p>	<p style="text-align: right;">专任教师岗位聘用委员会主任委员签名：_____</p> <p style="text-align: right;">____年____月____日</p>

备注：表格请用 A4 纸打印，与聘岗有关佐证材料附后。



Anomalous evolution of corrosion behaviour of warm-rolled type 304 austenitic stainless steel

Huimin Tao^{a,1}, Chengshuang Zhou^{a,1}, Yuanyuan Zheng^a, Yuanjian Hong^a, Jinyang Zheng^{b,*}, Lin Zhang^{a,*}

^a Institute of Material Forming and Control Engineering, Zhejiang University of Technology, Hangzhou 310014, China

^b Institute of Chemical Machinery Engineering, Zhejiang University, Hangzhou 310027, China

ARTICLE INFO

Keywords:

- A. Stainless steel
- B. Polarization
- B. EIS
- C. Pitting corrosion
- C. Intergranular corrosion

ABSTRACT

The effect of warm-rolling (at 200 °C) on the corrosion behaviour of type 304 steel in the 3.5% NaCl solution was investigated by electrochemical measurements and microstructural characterization. The pitting corrosion resistance of the specimens decreased with increasing deformation, reached the bottom at 20% deformation, and then improved with further deformation. The increase in low angle and low- Σ coincidence site lattice (CSL) grain boundaries improves the corrosion resistance, while the higher dislocation density weakens the corrosion resistance. The corrosion behaviour of warm-rolled austenitic stainless steel is determined by the interplay of the dislocation and grain boundary effects.

1. Introduction

Austenitic stainless steels are considered to be an important category of materials due to their suitable electrochemical stability, superior mechanical properties, ease of fabrication, abundance, and relatively low cost. Thus, austenitic stainless steels have been widely applied in such industries as the aerospace, automotive, and electronics industries [1–4]. However, the corrosion behaviour of austenitic stainless steels has been one of the main factors preventing their further applications. Corrosion resistance is one of the most important criteria for evaluating the performance of austenitic stainless steels in corrosive environments. Numerous researchers [5–7] have reported on the corrosion behaviour of austenitic stainless steels in corrosive environments. Despite the intrinsic higher corrosion resistance of austenitic stainless steels, they are extremely susceptible to local corrosion, such as the pitting or intergranular corrosion in severe corrosive environments, such as chloride and alkaline solutions [8–11]. Therefore, for further applications, it is crucial to study the corrosion susceptibility of austenitic stainless steel.

The pre-deformation of stainless steels is unavoidable during the fabrication processes, such as rolling, extrusion, shot peening, ultrasonic peening, and surface mechanical attrition treatment. Rolling, a traditional metallurgical process for improving the mechanical properties of the materials, has been widely used in materials processing.

The plastic deformation induced by rolling or the other afore mentioned methods is likely to not only modify the microstructure but also change the mechanical properties of stainless steels [12,13]. Numerous studies [14–16] have been carried out on the evolution of texture or microstructure in cold-rolling stainless steels. It was reported that mechanical twins, phase transformation and dislocations developed during the rolling process in austenitic stainless steels. The microstructure induced by rolling depends on the material composition, deformation temperature, and degree of deformation. The changes in the microstructure may have a significant effect on the corrosion behaviour of materials. Nam et al. [17] reported that the oriented low-energy grain boundaries induced by the rolling process increased the corrosion resistance of the low alloy steel. Peguet et al. [18] showed that cold-rolling improved the pit propagation rate of type 304 steel and weakened its repassivation ability due to dislocation pile-ups. Xiang [19] also reported that the corrosion resistance of the LA51 alloy sheet improved due to its characteristic textures, texture intensity, and the formation of twins and protective surface films during the rolling process. Similar results have also been reported by Huang [20] and Shakhova [21].

However, in metastable stainless steels, the evolution of microstructure induced by warm-rolling is notably different from that induced by cold-rolling. Warm-rolling at a higher temperature can suppress the strain-induced α' martensitic transformation in these stainless steels. Additionally, warm-rolling can decrease the rolling resistance

* Corresponding authors.

E-mail addresses: zhlin@zjut.edu.cn (J. Zheng), jyjh@zju.edu.cn (L. Zhang).

¹ These authors contributed equally to this work.

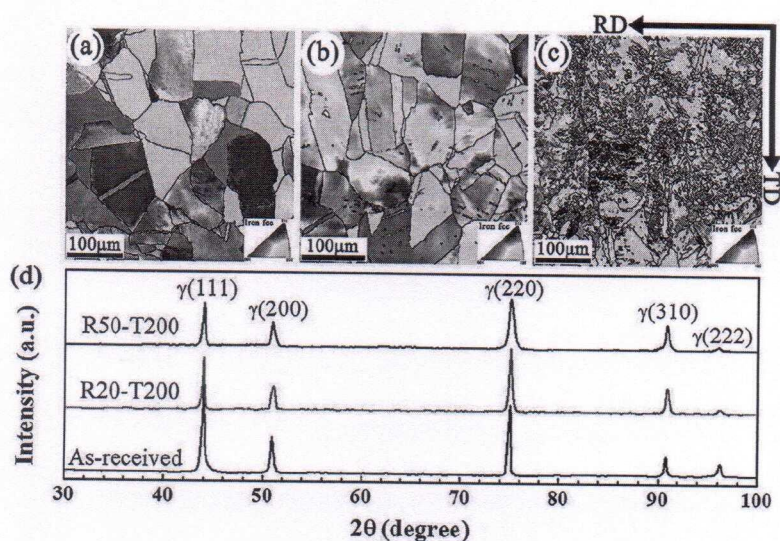


Fig. 1. IPF maps and XRD results of type 304 steel with different deformation percentages: (a) as-received, (b) R20-T200, (c) R50-T200, (d) XRD results. (RD: rolling direction, TD: transverse direction).

force and improve the plasticity of the steel compared with cold-rolling [22]. Such microstructural changes in warm-rolled stainless steels may have a significant impact on the corrosion resistance of the steels. However, the evolution of microstructure induced by warm-rolling has not been thoroughly elucidated to date, and the relationship between the corrosion behaviour and warm-rolling has not been investigated to date in austenitic stainless steels.

In this work, the effects of the rolling temperature of 200 °C (0.14 T_m , T_m : the melting temperature of 304 austenitic stainless steel) and rolling deformation percentage (10–50%) on the corrosion behaviour of type 304 steel in the 3.5 wt.% NaCl solution were investigated by various electrochemical measurements. Anomalous evolution of the corrosion behavior of warm-rolled type 304 steel was observed, and the mechanism for pitting corrosion was discussed based on the microstructural changes induced by warm-rolling.

2. Experimental

The base type 304 stainless steel (0.07 wt.% C, 0.33 wt.% Si, 1.13 wt.% Mn, 18.09 wt.% Cr, 8.06 wt.% Ni, 0.022 wt.% S, 0.039 wt.% P) plates were solution-treated at 1050 °C for 1 h and then were water quenched to obtain a homogeneous microstructure. Warm-rolling was conducted under isothermal conditions, where both the roller and specimens were preheated to 200 °C. The plates were multi-step unidirectionally rolled with a reduction of approximately 1% of their initial thickness during each pass, until the desired deformation percentage (10–50%) was achieved after numerous successive passes. Henceforth, the obtained specimens will be referred to as the RXX-T200 specimen. For example, the R20-T200 specimen is the specimen rolled at 200 °C to obtain a 20% reduction of its initial thickness.

The plate specimens for electrochemical measurements were cut parallel to the rolling direction, and then machined into test samples with the dimensions of 10 mm × 10 mm × 2 mm. The rear surfaces were connected using an insulated copper wire and sealed with a curing epoxy resin to avoid crevice corrosion. The surfaces of the specimens were successively ground with emery papers up to 2000 grit and polished with a 0.1 μm diamond polishing agent. All of the specimens were rinsed with deionized water and acetone and dried immediately prior to testing. Electrochemical measurements were conducted using an IVIUMSTAT electrochemical workstation equipped with the corrosion software of Ivium Soft. A three-electrode cell was used for the electrochemical measurements, including a platinum sheet (as the

counter electrode), a saturated calomel electrode (SCE, as the reference electrode), and the specimens prepared as described above (as the working electrode). The electrode potentials were measured and are presented in reference to the SCE scale. Electrochemical experiments were conducted in a 3.5 wt.% NaCl solution at 25 ± 1 °C. The specimens were immersed in the solution for 10 min to attain a stable reaction system prior to testing. The open-circuit potential (E_{oc}) value was measured in the 3.5 wt.% NaCl solution for 3600 s. Potentiodynamic polarization measurements were conducted at a scanning rate of 1 mV/s from $-0.6 V_{SCE}$ to $+1 V_{SCE}$. For the potentiostatic polarization, the current density was recorded at a constant potential of $+100 mV_{SCE}$ for 6000 s. Prior to the electrochemical impedance spectroscopy (EIS) tests, the specimens were immersed in the solution with a constant potential of $+100 mV_{SCE}$ (the potential was obtained from the passive region of the polarization curves) for 2 h to form the passive film. EIS measurements were carried out at the open-circuit potential with a signal amplitude perturbation voltage of $10 mV_{SCE}$ over the frequency range of 100 kHz–10 mHz. Each experiment was repeated at least three times under identical conditions to confirm the reproducibility of the tests. Subsequent heat-treatments for the specimens were conducted at 400 °C (0.29 T_m) for 4 h, 500 °C (0.36 T_m) for 4 h, and 950 °C (0.68 T_m) for 1 h, respectively, and the specimens treated at 400 °C and 500 °C were then furnace cooled, while the specimens treated at 950 °C were water cooled. All of the specimens were annealed in vacuum atmosphere. Intergranular corrosion tests [23,24] of the specimens were evaluated by the oxalic acid electrolytic corrosion with a current density of $1 A cm^{-2}$ for 90 s.

The microstructures of the specimens were observed by electron backscatter diffraction (EBSD), X-ray diffraction (XRD) and optical microscope (OM).

3. Results

3.1. Microstructure characterization

The inverse pole figure (IPF) maps and XRD results for the type 304 stainless steel specimens with different warm-rolling deformation percentages are shown in Fig. 1. The as-received specimen exhibited irregular austenitic grains with some annealing twins after the solution-treatment as shown in Fig. 1(a). The R20-T200 specimen had a polygonal microstructure similar to that of the as-received specimen, as shown in Fig. 1(b). The grain sizes and grain morphologies of the as-

received and R20-T200 specimens were similar, implying that the 20% deformation slightly altered the microstructure. However, the original grain boundaries almost disappeared, and the microstructure changed greatly as the deformation increased to 50%, as shown in Fig. 1(c). These results may be attributed to the dislocation pile-ups around the grain boundaries that constrain the deformation of austenite during the deformation process [25]. In addition, heterogeneous grain clusters were observed in some original grains, and the grains orientation became more disordered with increasing deformation, particularly for the R50-T200 specimen. The original grain boundaries became fairly blurry or even disappeared, resulting in a large amount of incomplete grains in the R50-T200 specimen.

The XRD patterns for the as-received and warm-rolled specimens are shown in Fig. 1(d). The γ (111), γ (200), γ (220), γ (310), and γ (222) diffraction peaks are due to type 304 steel in the austenite phase. The XRD results indicated that warm-rolling did not lead to any phase transitions in type 304 steel. Additionally, the heights of the XRD peaks decreased with increasing deformation, which may be attributed to the greater amount of defects and greater distortion of the crystal structures generated during the deformation process.

3.2. Open-circuit potential

The open-circuit potential (E_{ocp}) curves of the as-received and warm-rolled specimens are displayed in Fig. 2. The E_{ocp} values of all specimens decreased in the first approximately 250 s and then reached a stable level after approximately 1800 s, as shown in Fig. 2. This finding may explain the observation that the specimens should be immersed in the solution for some time prior to the experiments, and with a longer immersion time resulting in a more stable surface. However, significant changes were observed in E_{ocp} stable values for various warm-rolling deformation percentages. It is observed that the warm-rolled specimens showed considerably lower E_{ocp} values in the 3.5 wt.% NaCl solution than the as-received specimen. The E_{ocp} value of the R20-T200 specimen (-0.223 V_{SCE}) clearly decreased compared with that of the as-received specimen (-0.137 V_{SCE}). When the deformation was above 20%, the E_{ocp} value increased slightly with further deformation. The E_{ocp} behaviour is closely related to the change in the passivation state of the stainless steel [8]. The lower E_{ocp} value indicates poor passivation state of the stainless steel with the degraded passive film and vice versa. The deteriorated passive film can increase the corrosion rate of the specimen. Thus, the above results indicate that warm-rolling increased the corrosion rate of the type 304 steel in the 3.5 wt.% NaCl solution. The corrosion rate reached the highest value at 20% deformation and then decreased with further deformation.

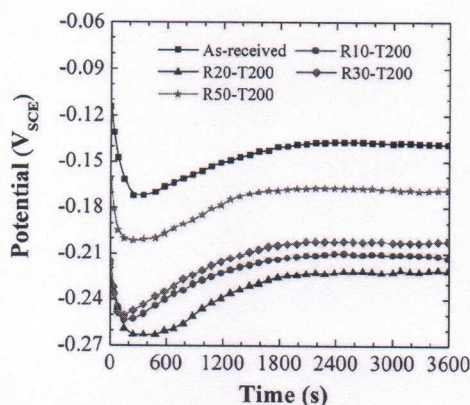


Fig. 2. Open-circuit potential curves of the as-received and warm-rolled specimens.

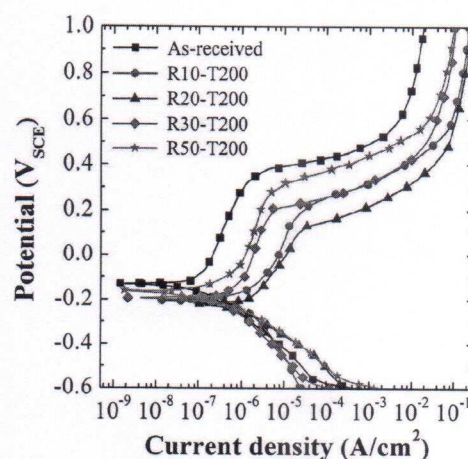


Fig. 3. Potentiodynamic polarization curves of the as-received and warm-rolled specimens.

3.3. Potentiodynamic polarization

Potentiodynamic polarization behaviour of the as-received and warm-rolled specimens are shown in Fig. 3. While all of the curves are similar to each other, a noticeable effect of warm-rolling is observed, indicating that warm-rolling may influence the corrosion process. To reveal the corrosion behaviour of the warm-rolled specimens, several related parameters, such as the corrosion potential (E_{corr}), corrosion current density (i_{corr}), passive current density (i_{pass}), pitting potential (E_{pit}), and cathodic Tafel slope (β_c), were obtained from Fig. 3 or from the Tafel extrapolation method [26], with the obtained values shown in Table 1. The i_{pass} value was obtained from the polarization curves in the middle of the passive region.

All of the specimens exhibited a cathodic shift in E_{corr} , with the E_{corr} values of the as-received, R10-T200, R20-T200, R30-T200, and R50-T200 specimens in the 3.5 wt.% NaCl solution reaching -131.4 mV_{SCE} , -206.8 mV_{SCE} , -219.3 mV_{SCE} , -194.5 mV_{SCE} , and -159.4 mV_{SCE} , respectively. E_{corr} decreased with increasing deformation, reached the lowest value at 20% deformation, and then increased with further deformation. Theoretically, a higher E_{corr} indicates a higher chemical inertness and better corrosion resistance for preventing the anodic process [27]. Thus, the general corrosion resistance of all the specimens followed the order of as-received > R50-T200 > R30-T200 > R10-T200 > R20-T200. In addition, type 304 steel presented an obvious passivation in the 3.5 wt.% NaCl solution. The existence of a larger passivation region indicates that a more protective passive film was formed on the specimen surface. The i_{pass} of the R20-T200 specimen ($7.664 \mu\text{A cm}^{-2}$) was considerably larger than that of the as-received specimen ($0.367 \mu\text{A cm}^{-2}$). i_{pass} reflects the dissolution rate of the passive film during the corrosion process such that a larger i_{pass} indicates a higher dissolution rate [28,29]. The E_{pit} value of the R20-T200 specimen was considerably smaller than that of the as-received specimen but increased for the deformation above 20%. Thus, warm-rolling could distinctly increase the pitting susceptibility in type 304 steel, particularly for the R20-T200 specimen. With a further increase of warm-rolling deformation, the pitting susceptibility first increased and then decreased.

The surface morphologies of the as-received and warm-rolled specimens after the potentiodynamic polarization are shown in Fig. 4(a)–(e). The density of corrosive pits on the specimen surfaces increased after warm-rolling, particularly for the R20-T200 specimen. An examination of the micrographs also demonstrated that warm-rolling promoted the pitting corrosion of type 304 steel. The corrosive pits became elongated along the rolling direction with an increase in deformation percentage. On the other hand, as shown in

Table 1

Electrochemical parameters of the as-received and warm-rolled specimens. E_{corr} : corrosion potential, i_{corr} : corrosion current density, i_{pass} : passive current density, E_{pit} : pitting potential, β_c : cathodic Tafel slope.

Specimens	E_{corr} (mV _{SCE})	i_{corr} (nA cm ⁻²)	i_{pass} (μA cm ⁻²)	E_{pit} (mV _{SCE})	β_c (mV decade ⁻¹)
As-received	-131.4 ± 3.5	1.436 ± 0.14	0.367 ± 0.02	404.6 ± 5.2	-285.2 ± 25.9
R10-T200	-206.8 ± 4.1	12.501 ± 0.51	7.357 ± 0.04	187.5 ± 5.9	-370.2 ± 46.5
R20-T200	-219.3 ± 3.3	69.470 ± 3.48	7.664 ± 0.03	131.1 ± 1.7	-376.8 ± 21.1
R30-T200	-194.5 ± 3.7	2.174 ± 0.05	1.547 ± 0.03	218.3 ± 5.2	-361.3 ± 32.5
R50-T200	-159.4 ± 4.5	1.807 ± 0.04	1.503 ± 0.04	332.4 ± 6.3	-339.1 ± 31.8

Fig. 4(a1)–(e1), tiny corrosive pits were initiated at the grain boundary in all of the specimens at the anodic potentials of E_{pit} , demonstrating that the grain boundary was the preferential initiation site for the corrosive pits. Therefore, grain boundaries may play the primary role in the pitting corrosion of warm-rolling type 304 steel, while a small number of inclusions may have little effect on the pitting corrosion.

Potentiodynamic polarization parameters and surface morphologies indicate the reduction of the corrosion resistance in the warm-rolled 304 specimens. The corrosion resistance decreased with increasing deformation, reached the bottom at 20% deformation, and then increased with further deformation.

3.4. Potentiostatic polarization

The potentiostatic polarization curves of the as-received and warm-rolled specimens are shown in Fig. 5. The current densities of the specimens initially decreased and then stabilized at a low positive current density due to the formation of the passive film. During long term-operation, the current densities of the warm-rolled specimens were considerably higher and showed greater fluctuations than the current density of the as-received specimen, particularly for the R20-T200 specimen. As shown in the inset of Fig. 5, some current fluctuation spikes are observed above the baseline current due to the unstable passive films formed on the specimen surfaces. The frequency and height of the current fluctuation spikes of the warm-rolled specimens

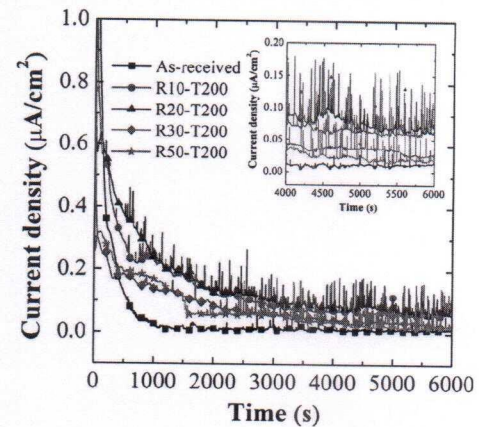


Fig. 5. Potentiostatic polarization curves of the as-received and warm-rolled specimens. The inset shows the magnified view of the curves from 4000 to 6000 s.

increased compared with that of the as-received specimen, particularly for the R20-T200 specimen, but then decreased with further increase in the deformation. Generally, the larger and more fluctuating current density reflects the thinner and porous film structure; such a film increases the opportunity of deleterious ions diffusion to accelerate the

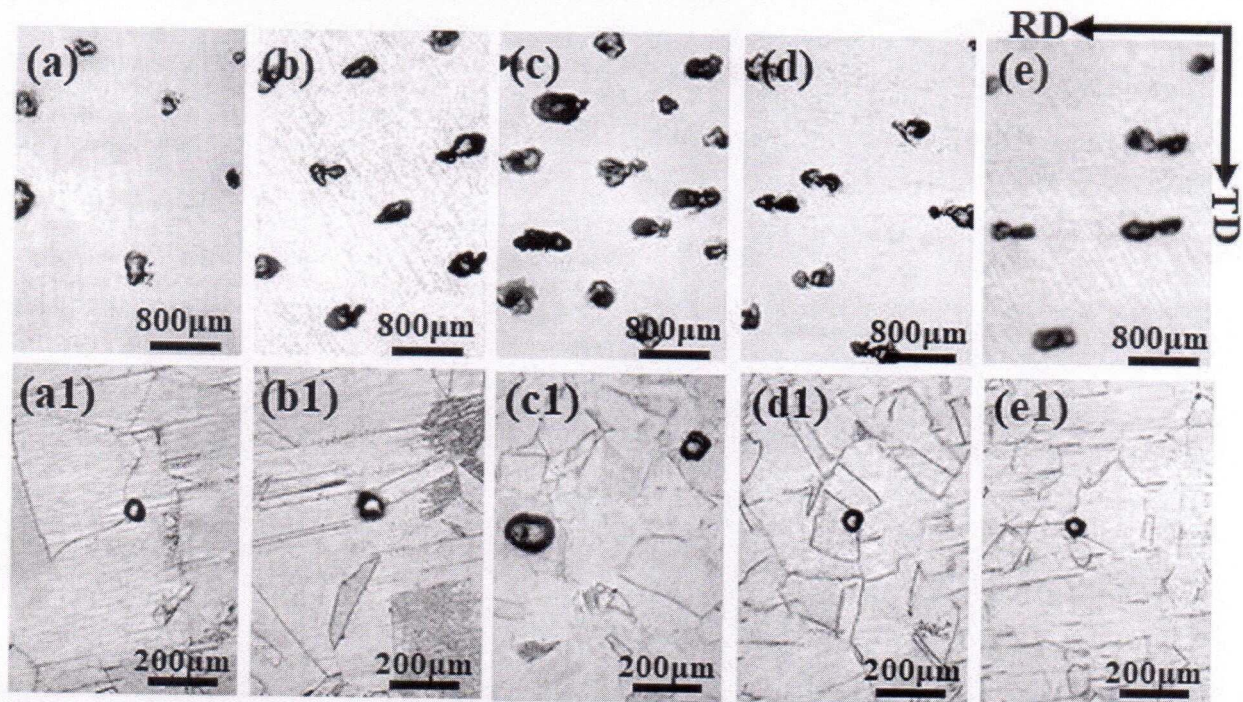


Fig. 4. Surface morphologies of the as-received and warm-rolled specimens after the potentiodynamic polarization measurements (a–e) and beyond the pitting potential (a1–e1). (a,a1): as-received, (b,b1): R10-T200, (c,c1): R20-T200, (d,d1): R30-T200, and (e,e1): R50-T200. (RD: rolling direction, TD: transverse direction).

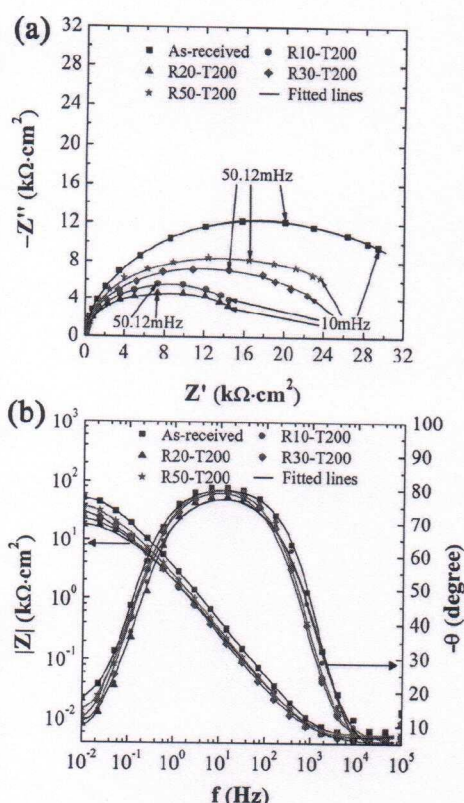


Fig. 6. Nyquist plots (a) and Bode plots (b) of the as-received and warm-rolled specimens.

electrochemical reaction [30]. The deteriorated passive film formed by warm-rolling increased the corrosion rate of the specimens. As a result, the corrosion rate increased with increasing deformation, reached the highest value at 20% deformation, and then decreased with further deformation.

3.5. Electrochemical impedance spectroscopy

The Nyquist and Bode plots obtained by EIS for the as-received and warm-rolled specimens are shown in Fig. 6(a) and (b), respectively. All of the specimens presented the specific capacitive semicircles over the entire measurement frequency region in Fig. 6(a), indicating that warm-rolling did not alter the corrosion mechanism of type 304 steel. Theoretically, the diameter of the capacitive semicircle arc provides an indication for the corrosion resistance of the films, and the larger semicircle arc diameter indicates the higher corrosion resistance of the films [31]. Warm-rolled specimens with the smaller semicircle arc diameters reflected the poor corrosion resistance of the passive films. In addition, the corrosion resistance of the passive films significantly decreased at 20% deformation and then increased with further deformation.

A maximum phase angle (approximately -80°) was observed over a certain frequency range in Fig. 6(b), representing a non-ideal capacitor of the type 304 steel. The specimen with the higher maximum phase angle will have the greater tendency of capacitive behaviour [32]. The maximum phase angles of the warm-rolled specimens, particularly for the R20-T200 specimen, were lower than that of the as-received specimen, indicating the smaller tendency of the capacitive behaviour of the warm-rolled specimens. On the other hand, the lower frequency region reflects the processes of the passive film stability, Warburg diffusion, and Faradic reactions [32–35]. The decrease in the phase angle observed at lower frequency region is due to the dissolution of the passive film. Generally, the phase angle at 0.01 Hz was compared for an

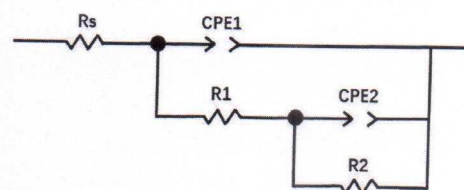


Fig. 7. Equivalent circuit model used to fit the impedance spectroscopy of the as-received and warm-rolled specimens in 3.5 wt.% NaCl solution.

effective analysis of the corrosion protective ability of the specimens. The warm-rolled specimens showed lower phase angle (at 0.01 Hz) compared with that of the as-received specimen, indicating the poor corrosion protective ability of the warm-rolled specimens.

Numerous models have been proposed for interpreting the impedance spectra results for metals [36–39]. The equivalent circuit model in Fig. 7 was used for fitting the EIS from the above data. In this model, the passive films formed on the specimens were considered to have capacitive characteristics. Constant phase element (CPE) was used in the fitting procedure to reflect the frequency dispersion behaviour of the physical phenomena [40–43] and was defined as [37]:

$$Z(\omega) = Z_0 \cdot (i\omega)^{-n} \quad (1)$$

where Z_0 is the proportional factor, ω is the angular frequency, and n is the CPE exponent corresponding to the phase shift. In this model, R_s is the electrolyte resistance between the reference and working electrodes. R_1 and R_2 are the passive film and charge transfer resistances, respectively, and CPE_1 and CPE_2 are their corresponding constant phase elements. In addition, C_1 and C_2 are their corresponding capacitance values calculated by Brug's formula [44,45]. EIS fitting parameters details are plotted in Fig. 6 and are presented in Table 2. R_s remained almost constant, indicating the similar ion conductivity in the 3.5 wt.% NaCl solution and the good reproducibility of the experiments. The warm-rolled specimens showed relatively lower R_1 and R_2 values compared with those of the as-received specimen, particularly for the R20-T200 specimen, indicating the weaker protective ability of the passive film formed on the surfaces of the warm-rolled specimens. In addition, the CPE_1 and CPE_2 values of the warm-rolled specimens increased compared with those of the as-received specimen, suggesting the presence of defect in the passive film and the higher reaction rate that were caused by warm-rolling. The lower n value of the warm-rolled specimens also represented the poor capacitive behaviour of the passive film. The laws of the calculated C_1 and C_2 values were in agreement with the fitted results of EIS. Thus, warm-rolling decreased the corrosion resistance of type 304 steel due to the formation of the thinner and porous passive film on the specimen surface. The corrosion resistance of the passive film decreased with increasing deformation, reached the bottom at 20% deformation, and then increased with further deformation. These results are in agreement with the results of the other electrochemical measurements.

3.6. Intergranular corrosion

The surface morphologies of as-received and warm-rolled specimens after the intergranular corrosion tests are shown in Fig. 8. Apparently, the degree of the grain boundary corrosion decreased with increasing deformation with or without annealing. As shown in the insets of Fig. 8, the corrosion grooves of the grain boundaries become fairly thin and blurred or even disappeared with increasing deformation. Grain boundaries became disordered, and the connectivity of the grain boundary network was interrupted significantly as the deformation reached 50%. After annealing at 950°C , the extent of the grain boundary corrosion of the R50-T200 specimen decreased slightly due to the decrease in dislocation density.

Table 2

Fitted electrochemical parameters of the impedance spectra for the as-received and warm-rolled specimens in 3.5 wt.% NaCl solution.

Specimens	$R_s (\Omega \text{ cm}^2)$	$CPE_1 (\Omega^{-1} \text{ cm}^{-2} \text{ s}^n)$	n_1	$R_1 (\Omega \text{ cm}^2)$	$C_1 (\text{F cm}^{-2})$	$CPE_2 (\Omega^{-1} \text{ cm}^{-2} \text{ s}^n)$	n_2	$R_2 (\Omega \text{ cm}^2)$	$C_2 (\text{F cm}^{-2})$	χ^2
As-received	5.499	5.384×10^{-5}	0.914	2.512×10^4	1.250×10^{-5}	3.202×10^{-4}	0.909	9.450×10^3	8.714×10^{-4}	5.631×10^{-4}
R10-T200	5.523	9.306×10^{-5}	0.876	1.551×10^4	1.632×10^{-4}	1.100×10^{-3}	0.787	3.936×10^3	1.002×10^{-2}	4.863×10^{-4}
R20-T200	5.346	9.604×10^{-5}	0.870	1.477×10^4	1.733×10^{-4}	1.918×10^{-3}	0.771	1.138×10^3	1.820×10^{-2}	4.285×10^{-4}
R30-T200	5.303	9.101×10^{-5}	0.901	1.619×10^4	2.332×10^{-5}	3.747×10^{-4}	0.827	4.211×10^3	2.694×10^{-3}	1.813×10^{-3}
R50-T200	5.765	7.178×10^{-5}	0.908	1.676×10^4	2.046×10^{-5}	3.950×10^{-4}	0.878	7.841×10^3	1.575×10^{-3}	6.221×10^{-4}

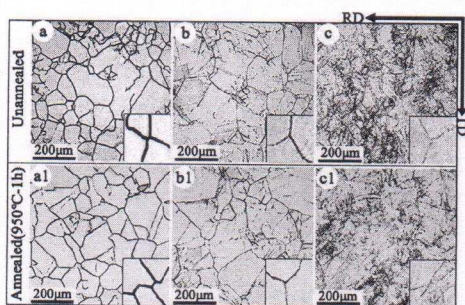


Fig. 8. Surface morphologies of the as-received and warm-rolled specimens unannealed and annealed at 950 °C for 1 h after intergranular corrosion. a: as-received, a1: as-received-950; b: R20-T200, b1: R20-T200-950; c: R50-T200, c1: R50-T200-950. (RD: rolling direction, TD: transverse direction).

4. Discussion

The experimental results described above suggested that the corrosion resistance of type 304 steel decreased with increasing warm-rolling deformation, reached the bottom at 20% deformation, and then improved with further deformation. The electrochemical parameters of the specimens obtained by open-circuit potential (Fig. 2), potentiodynamic polarization (Fig. 3), potentiostatic polarization (Fig. 5), and EIS (Fig. 6) experiments and the surface morphologies (Fig. 4) corroborate each other. It is well-known that the corrosion resistance of the materials depends on their composition and microstructure; thus, the microstructural evolution induced by warm-rolling may play an important role in the corrosion behaviour of type 304 steel.

Subsequent heat-treatments were conducted to study the relationship between the microstructure and corrosion behaviour of type 304 steel. To eliminate the residual stress caused by warm-rolling, the specimens were annealed at 400 °C for 4 h, and the corresponding potentiodynamic polarization curves were shown in Fig. 9. The E_{corr} values of the as-received-400, R20-T200-400, and R50-T200-400

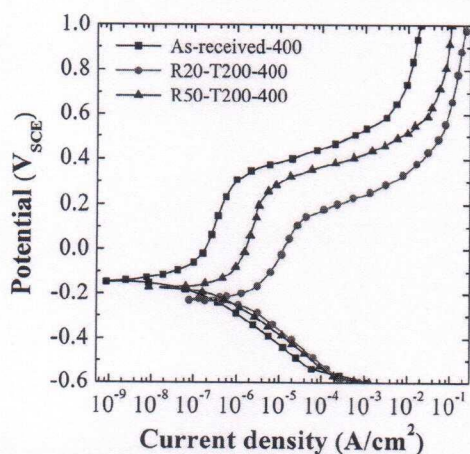


Fig. 9. Potentiodynamic polarization curves of the as-received and warm-rolled specimens after annealing at 400 °C for 4 h.

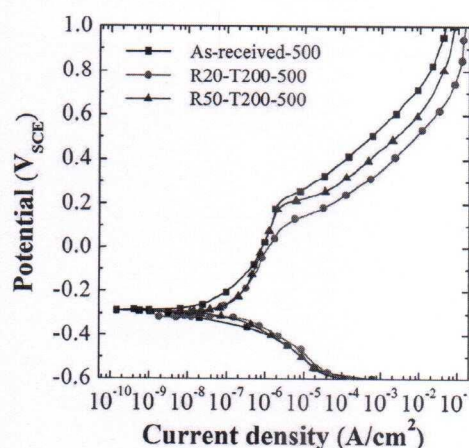


Fig. 10. Potentiodynamic polarization curves of the as-received and warm-rolled specimens after annealing at 500 °C for 4 h.

specimens were $-148.5 \text{ mV}_{\text{SCE}}$, $-226.3 \text{ mV}_{\text{SCE}}$ and $-172.7 \text{ mV}_{\text{SCE}}$, respectively. The E_{pit} values of the specimens were $374.6 \text{ mV}_{\text{SCE}}$, $146.7 \text{ mV}_{\text{SCE}}$ and $284.7 \text{ mV}_{\text{SCE}}$, respectively. The electrochemical parameters were similar to those of the unannealed specimens, as shown in Figs. 3 and 9. Thus, annealing at 400 °C had little effect on the corrosion resistance of the warm-rolled specimens, indicating that the residual stress was not the main factor affecting the corrosion resistance of the warm-rolled type 304 steel.

As shown in Fig. 10, after annealing at 500 °C, the E_{corr} values of the as-received-500, R20-T200-500, and R50-T200-500 specimens were $-286.4 \text{ mV}_{\text{SCE}}$, $-314.7 \text{ mV}_{\text{SCE}}$, and $-292.9 \text{ mV}_{\text{SCE}}$, respectively. The E_{pit} values of these specimens were $250.5 \text{ mV}_{\text{SCE}}$, $131.7 \text{ mV}_{\text{SCE}}$, and $221.7 \text{ mV}_{\text{SCE}}$, respectively. Thus, the corrosion resistance of the 500 °C annealed specimens was distinctly decreased compared with those of the unannealed or 400 °C annealed specimens. The decrease in the corrosion resistance of the 500 °C annealed specimens may be attributed to the sensitization induced by the heat treatment. Sensitization of austenitic stainless steels has been studied by some researchers [46–49].

Furthermore, the specimens were annealed at 950 °C for 1 h to reduce the dislocations and the corresponding potentiodynamic polarization curves are shown in Fig. 11. The E_{corr} values increased from $-138.7 \text{ mV}_{\text{SCE}}$ (as-received-950) to $-73.6 \text{ mV}_{\text{SCE}}$ (R50-T200-950) with further deformation. The i_{pass} of the R50-T200-950 specimen ($0.098 \mu\text{A cm}^{-2}$) was considerably smaller than that of the as-received-950 specimen ($0.313 \mu\text{A cm}^{-2}$). The E_{pit} values of the as-received-950, R20-T200-950, and R50-T200-950 specimens reached approximately $384.5 \text{ mV}_{\text{SCE}}$, $429.6 \text{ mV}_{\text{SCE}}$, and $518.9 \text{ mV}_{\text{SCE}}$, respectively. Thus, the corrosion resistance of the warm-rolled specimens annealed at 950 °C improved distinctly compared with these of the unannealed specimens. Additionally, the extent of the grain boundary corrosion of the specimens decreased after annealing at 950 °C, as shown in Fig. 8(a1)–(c1). Thus, the dislocation pile-ups caused by deformation decreased the corrosion resistance of type 304 steel, as was also confirmed by previous studies [50–52]. The pitting corrosion resistance of the 950 °C annealed specimens followed the order of R50-T200-950 > R20-T200-

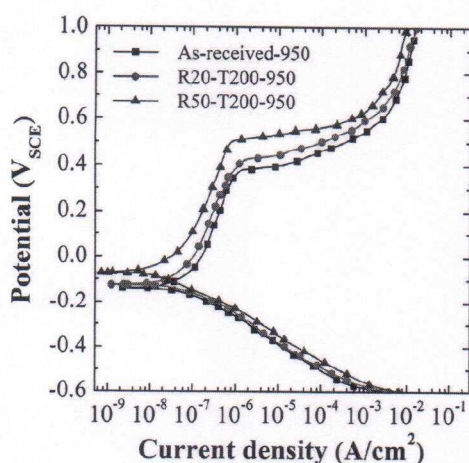


Fig. 11. Potentiodynamic polarization curves of the as-received and warm-rolled specimens after annealing at 950 °C for 1 h.

950 > as-received-950. The pitting corrosion resistance improved with increasing deformation, unlike the trend observed in unannealed or 400 °C annealed specimens. On the other hand, the pits were preferentially initiated at the grain boundaries, as shown in Fig. 4(a1)–(e1). Therefore, the grain boundaries may play the decisive role in the corrosion susceptibility of the warm-rolled type 304 steel.

How does the grain boundary change by warm-rolling? The grain boundaries with a misorientation of less than approximately 15° were classified as the low angle grain boundaries (green line) and the grain boundaries with a misorientation of above 15° were classified as the high angle grain boundaries (black line), as shown in Fig. 12(a) and (b). The warm-rolled specimens showed a heterogeneous distribution of grain clusters that contained a large number of low angle grain

boundaries. These heterogeneous low angle grain boundaries were distributed around the high angle grain boundaries in the R20-T200 specimen (Fig. 12a), while they covered the entire observation area in the R50-T200 specimen (Fig. 12b). The dissolution of the original high angle grain boundaries and a marked increase in low angle grain boundaries were observed with increasing deformation. On the other hand, the coincidence site lattice (CSL) grain boundaries with $\Sigma \leq 29$ were classified as the low- Σ CSL grain boundaries (red, yellow, green, and blue lines), as shown in Fig. 12(a1) and (b1). The CSL grain boundaries with $\Sigma > 29$ were classified as the random grain boundaries (black line) based on the Brandon criterion [53]. Most of the low- Σ CSL grain boundaries belong to the $\Sigma 3$ grain boundaries (red line) in addition to a small amount of other low- Σ CSL grain boundaries. Clearly, the amount of the low- Σ CSL grain boundaries increased with increasing deformation. A fraction of the random grain boundaries were replaced by the low- Σ CSL grain boundaries, while the others were still preserved. The low- Σ CSL grain boundaries replacing the random grain boundaries may interrupt the connectivity of the random grain boundary network [54–56]. The connectivity of the random grain boundary network in the R20-T200 specimen was better, but the random grain boundary network was severely interrupted in the R50-T200 specimen. The low- Σ CSL grain boundaries have a high fraction of jointed lattice points, and both the low angle and low- Σ CSL grain boundaries have the distinctly lower energy [57,58]; thus they show better corrosion resistance compared with the random grain boundary with these grain boundaries characters. The increase in these grain boundaries may prevent the primary stages of corrosion and improve the corrosion resistance of the material [59–61]. The amount of the original high angle grain boundaries decreased, while the low angle and low- Σ CSL grain boundaries increased, with increasing deformation, resulting in the improvement of the corrosion resistance of grain boundary. Although the grain boundary reactivity may vary greatly due to its crystallography and distributions, all types of grain boundaries are

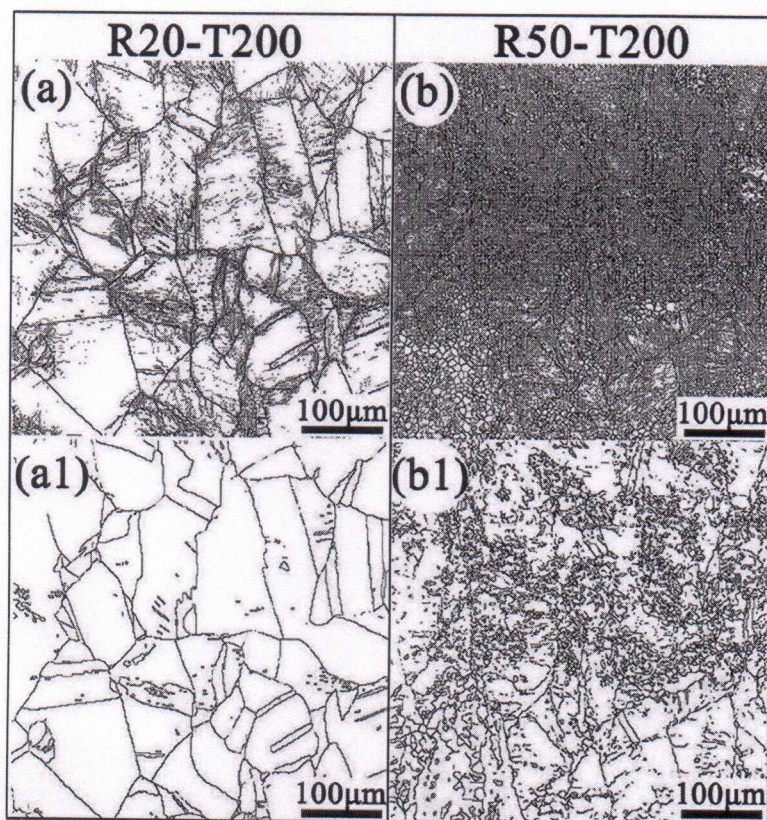


Fig. 12. EBSD maps of the distributions of grain boundaries for warm-rolled specimens: (a,b): the low angle and high angle grain boundaries maps, black lines indicate the high angle grain boundaries and green lines indicate the low angle grain boundaries; (a1,b1): the CSL grain boundaries maps, black lines indicate the random grain boundaries and other lines indicate the low- Σ CSL grain boundaries. (For interpretation of the references to colour in this figure legend, the reader is referred to the web version of this article.)

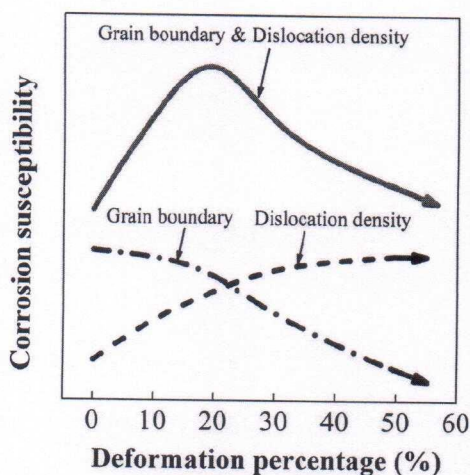


Fig. 13. Scheme of the dependence of corrosion susceptibility on the dislocation density and grain boundaries in the warm-rolled specimens.

more active than the grain bulk. The grain boundary is an important crystallographic defect with a disordered atomic arrangement and it promotes ion adsorption to accelerate the corrosion. Additionally, grain boundaries clearly decrease the electrical conductivity of polycrystalline metals [62,63] and are difficult to be passivated, decreasing the corrosion resistance of the material. The surface morphologies shown in Fig. 4(a1)–(e1) demonstrate the poor corrosion resistance of the grain boundary during corrosion process. Corrosion pits preferentially initiate at the grain boundary and are likely to develop into localized damage. The higher corrosion resistance of the grain boundary obtained by increasing deformation prevents the initiation and development of the corrosion pits and improves the pitting corrosion resistance of type 304 steel.

The changes in the dislocation density and grain boundary due to different warm-rolling deformation percentage significantly influence the initiation and development of corrosion pits. The dependence of corrosion susceptibility on dislocation density and grain boundary in the warm-rolled specimens is described in Fig. 13. The dislocation density, low angle and low- Σ CSL grain boundaries increased with increasing deformation. The increase in low angle and low- Σ CSL grain boundaries caused by warm-rolling improves the corrosion resistance, while the increase in dislocation density weakens the corrosion resistance. The corrosion behaviour of the warm-rolled type 304 steel is determined by the interplay of the dislocation and grain boundary effects, which is the main reason for the anomalous evolution of the corrosion behavior of warm-rolled type 304 steel. This work may help to elucidate the relationship between the microstructure and corrosion behaviour and will be valuable for optimizing the production and processing parameters of stainless steels for simultaneous enhancement of mechanical properties and corrosion resistance.

5. Conclusions

The effect of warm-rolling on the corrosion behaviour of type 304 steel in the 3.5 wt.% NaCl solution was investigated by electrochemical measurements and microstructural characterization. The main conclusions are as follows:

- (1) The corrosion resistance of the 304 specimens rolled at 200 °C decreased with increasing deformation, reached the bottom at 20% deformation, and then improved with further deformation.
- (2) Dislocation and grain boundary strongly influence the pitting corrosion of the warm-rolled 304 stainless steel, while the residual stress has little effect on it.
- (3) The increase in the low angle and low- Σ CSL grain boundaries

caused by warm-rolling improves the corrosion resistance, while the increase in the dislocation density weakens the corrosion resistance. The corrosion behaviour of the warm-rolled type 304 steel is determined by the interplay of the dislocation and grain boundary effects.

Acknowledgements

This research was supported by the National Key Basic Research Program of China (973 Program, Grant No. 2015CB057601), the National Natural Science Foundation of China (51571181) and the Zhejiang Provincial Natural Science Foundation of China (LY19E010006Q).

References

- [1] H. Luo, H. Su, C. Dong, K. Xiao, X. Li, Influence of pH on the passivation behaviour of 904L stainless steel bipolar plates for proton exchange membrane fuel cells, *J. Alloys Compd.* 686 (2016) 216–226.
- [2] H. Wang, M.A. Sweikart, J.A. Turner, Ferritic stainless steels as bipolar plate material for polymer electrolyte membrane fuel cells, *J. Power Sources* 115 (2003) 243–251.
- [3] Y. Yang, X. Ning, H. Tang, L. Guo, H. Liu, Effects of passive films on corrosion resistance of uncoated SS316L bipolar plates for proton exchange membrane fuel cell application, *Appl. Surf. Sci.* 320 (2014) 274–280.
- [4] K. Cho, W. Lee, S. Lee, H. Jang, Corrosion resistance of chromized 316L stainless steel for PEMFC bipolar plates, *J. Power Sources* 178 (2008) 671–676.
- [5] M. Domínguez-Aguilar, R. Newman, Detection of deleterious phases in duplex stainless steel by weak galvanostatic polarization in halide solutions, *Corros. Sci.* 48 (2006) 2560–2576.
- [6] A. Bautista, E. Paredes, S. Alvarez, F. Velasco, Welded, sandblasted, stainless steel corrugated bars in non-carbonated and carbonated mortars: a 9-year corrosion study, *Corros. Sci.* 102 (2016) 363–372.
- [7] M. Kaneko, H.S. Isaacs, Effects of Mo and Cr on pitting corrosion resistance of austenitic stainless steels in Br and Cl solutions, *J. Antimicrob. Chemother.* 20 (2011) 1–6.
- [8] M. Naghizadeh, D. Nakhaie, M. Zakeri, M.H. Moayed, The effect of dichromate ion on the pitting corrosion of AISI 316 stainless steel part II: pit initiation and transition to stability, *Corros. Sci.* 94 (2015) 420–427.
- [9] H. Luo, H.Z. Su, G.B. Ying, C.F. Dong, X.G. Li, Effect of cold deformation on the electrochemical behaviour of 304L stainless steel in contaminated sulfuric acid environment, *Appl. Surf. Sci.* 425 (2017) 628–638.
- [10] A.A. Aghuy, M. Zakeri, M.H. Moayed, Effect of grain size on pitting corrosion of 304L austenitic stainless steel, *Corros. Sci.* 94 (2015) 368–376.
- [11] X.L. Wei, C. Zhang, X. Ling, Effects of laser shock processing on corrosion resistance of AISI 304 stainless steel in acid chloride solution, *J. Alloys Compd.* 723 (2017) 237–242.
- [12] T.S. Byun, On the stress dependence of partial dislocation separation and deformation microstructure in austenitic stainless steels, *Acta Mater.* 51 (2003) 3063–3071.
- [13] H.W. Zhang, Z.K. Hei, G. Liu, J. Lu, K. Lu, Formation of nanostructured surface layer on AISI 304 stainless steel by means of surface mechanical attrition treatment, *Acta Mater.* 51 (2003) 1871–1881.
- [14] Z. Yanushkevich, A. Belyakov, R. Kaibyshev, Microstructural evolution of a 304-type austenitic stainless steel during rolling at temperatures of 773–1273 K, *Acta Mater.* 82 (2015) 244–254.
- [15] C. Donadille, R. Valle, P. Dervin, R. Penelle, Development of texture and microstructure during cold-rolling and annealing of F.C.C. alloys: example of an austenitic stainless steel, *Acta Metall.* 37 (1989) 1547–1571.
- [16] D. Raabe, Texture and microstructure evolution during cold rolling of a strip cast and of a hot rolled austenitic stainless steel, *Acta Mater.* 45 (1997) 1137–1151.
- [17] N.D. Nam, D.Y. Lee, J.G. Kim, N.J. Park, Effect of cold rolling on the corrosion properties of low-alloy steel in an acid-chloride solution, *Met. Mater. Int.* 20 (2014) 469–474.
- [18] L. Peguet, B. Malki, B. Baroux, Influence of cold working on the pitting corrosion resistance of stainless steels, *Corros. Sci.* 49 (2007) 1933–1948.
- [19] Q. Xiang, B. Jiang, Y. Zhang, X.B. Chen, J.F. Song, J.Y. Xu, L. Fang, F.S. Pan, Effect of rolling-induced microstructure on corrosion behavior of an as-extruded Mg-5Li-1Al alloy sheet, *Corros. Sci.* 119 (2017) 14–22.
- [20] J.X. Huang, Y.E. Xiao-Ning, X.U. Zhou, Effect of cold rolling on microstructure and mechanical properties of AISI 301LN metastable austenitic stainless steels, *J. Iron Steel Res. Int.* 19 (2012) 59–63.
- [21] Y.E. Shakhova, Z.C. Yanushkevich, A.N. Belyakov, Effect of cold rolling on the structure and mechanical properties of austenitic corrosion-resistant 10Kh18N8D3BR steel, *Russ. Metall.* 9 (2012) 772–778.
- [22] X.Y. Chen, C.S. Zhou, J.Y. Zheng, L. Zhang, Effects of α' martensite and deformation twin on hydrogen-assisted fatigue crack growth in cold/warm-rolled type 304 stainless steel, *Int. J. Hydrogen Energy* 43 (2018) 3342–3352.
- [23] M. Martin, H. Ludmila, S. Milan, V. Vlastimil, D. Catherine, G. Jacques, S. Zuzana, T. Ludek, Intergranular corrosion of AISI 316L steel, *Mater. Charact.* 46 (2001) 203–210.

- [24] T. Kuníková, H. Wendrock, K. Wetzg, D. Hrivňáková, EBSD investigation of intergranular corrosion attack on low interstitial stainless steel, *Mater. Corros.* 55 (2004) 437–443.
- [25] M. Breda, K. Brunelli, F. Grazzi, A. Scherillo, I. Calliari, Effects of cold rolling and strain-induced martensite formation in a SAF 2205 duplex stainless steel, *Metall. Mater. Trans. A* 46 (2015) 577–586.
- [26] M.A. Amin, K.F. Khaled, S.A. Fadl-Allah, Testing validity of the Tafel extrapolation method for monitoring corrosion of cold rolled steel in HCl solutions-experimental and theoretical studies, *Corros. Sci.* 52 (2010) 140–151.
- [27] Y. Zhao, L. Wei, P.Y. Yi, L.F. Peng, Influence of Cr-C film composition on electrical and corrosion properties of 316L stainless steel as bipolar plates for PEMFCs, *Int. J. Hydrogen Energy* 41 (2016) 1148–1149.
- [28] J.W. Schultze, M. Lohrengel, Stability, reactivity and breakdown of passive films. Problems of recent and future research, *Electrochim. Acta* 45 (2000) 2499–2513.
- [29] Y. Fu, X. Wu, E.H. Han, W. Ke, K. Yang, Z. Jiang, Effects of cold work and sensitization treatment on the corrosion resistance of high nitrogen stainless steel in chloride solutions, *Electrochim. Acta* 54 (2009) 1618–1629.
- [30] G. Burstein, P. Pistorius, S. Mattin, The nucleation and growth of corrosion pits on stainless steel, *Corros. Sci.* 35 (1993) 57–62.
- [31] C.N. Cao, On the impedance plane displays for irreversible electrode reactions based on the stability conditions of the steady-state-II. One state variable besides electrode potential, *Electrochim. Acta* 35 (1990) 831–836.
- [32] T. Balusamy, M. James, S. Kumar, T.S.N. Sankara Narayanan, Corrosion resistant Ti alloy for sulphuric acid medium: suitability of Ti-Mo alloys, *Mater. Corros.* 62 (2011) 803–806.
- [33] L. Chen, N. Myung, P.T.A. Sumodjo, K. Nobe, A comparative electrodisolution and localized corrosion study of 2024Al in halide media, *Electrochim. Acta* 44 (1999) 2751–2764.
- [34] J.N. Balaraju, A. Srinivasan, G. Yoganandan, V.K. William Grips, K.S. Rajam, Effect of Mn/Mo incorporated oxide layer on the corrosion behavior of AA 2024 alloy, *Corros. Sci.* 53 (2011) 4084–4092.
- [35] S.L.D. Assis, S. Wolyne, I. Costa, Corrosion characterization of titanium alloys by electrochemical techniques, *Electrochim. Acta* 51 (2006) 1815–1819.
- [36] A. Kocijan, D.K. Merl, M. Jenko, The corrosion behaviour of austenitic and duplex stainless steels in artificial saliva with the addition of fluoride, *Corros. Sci.* 53 (2011) 776–783.
- [37] H. Luo, X.Z. Wang, C.F. Dong, K. Xiao, X.G. Li, Effect of cold deformation on the corrosion behavior of UNS31803 duplex stainless steel in simulated concrete pore solution, *Corros. Sci.* 124 (2017) 178–192.
- [38] E. Hug, R.P. Babu, I. Monnet, A. Etienne, F. Moisy, V. Pralong, N. Enikeev, M. Abramova, X. Sauvage, B. Radiguet, Impact of the nano structuration on the corrosion resistance and hardness of irradiated 316 austenitic stainless steels, *Appl. Surf. Sci.* 392 (2017) 1026–1035.
- [39] J.L. Lv, W.L. Guo, T.X. Liang, The effect of pre-deformation on corrosion resistance of the passive film formed on 2205 duplex stainless steel, *J. Alloys Compd.* 686 (2016) 176–183.
- [40] L. Freire, M.J. Carmezim, M.G.S. Ferreira, M.F. Montemor, The electrochemical behaviour of stainless steel AISI 304 in alkaline solutions with different pH in the presence of chlorides, *Electrochim. Acta* 56 (2011) 5280–5289.
- [41] J.L. Lv, H.Y. Luo, Electrochemical investigation of passive film in pre-deformation AISI 304 stainless steels, *Appl. Surf. Sci.* 263 (2012) 29–37.
- [42] M. BenSalah, R. Sabot, E. Triki, L. Dhoubi, Ph. Refait, M. Jeannin, Passivity of Sanicro28 (UNS N-08028) stainless steel in polluted phosphoric acid at different temperatures studied by electrochemical impedance spectroscopy and Mott-Schottky analysis, *Corros. Sci.* 86 (2014) 61–70.
- [43] J.L. Lv, H.Y. Luo, The effects of cold rolling temperature on corrosion resistance of pure iron, *Appl. Surf. Sci.* 317 (2014) 125–130.
- [44] G.J. Brug, A.L.G. Van Den Eeden, M. Sluyters-Rehbach, J.H. Sluyters, The analysis of electrode impedances complicated by the presence of a constant phase element, *J. Electroanal. Chem.* 176 (1984) 275–295.
- [45] A.C. Bastos, M.G.S. Ferreira, A.M.P. Simões, Effects of mechanical forming on the corrosion of electrogalvanised steel, *Corros. Sci.* 69 (2013) 87–96.
- [46] A.P. Majidi, M.A. Streicher, The double loop reactivation method for detecting sensitization in AISI 304 stainless steels, *Corrosion (Houston, TX, U.S.)* 40 (1984) 584–593.
- [47] A.P. Majidi, M.A. Streicher, Potentiodynamic reactivation method for detecting sensitization in AISI 304 and 304L stainless steels, *Corrosion (Houston, TX, U.S.)* 40 (2012) 393–408.
- [48] C.S. Kim, S.J. Moon, W.S. Kong, Effect of sensitization treatment on corrosion properties in austenitic stainless steel 304, *Mater. Sci. Forum* 857 (2016) 232–236.
- [49] P. Muri, F.V.V. Sousa, K.S. Assis, A.C. Rocha, O.R. Mattos, I.C.P. Margarit-Mattos, Experimental procedures and sensitization diagnostics of AISI304 steel by double loop electrochemical potentiodynamic reactivation method, *Electrochim. Acta* 124 (2014) 183–189.
- [50] L. Peguet, B. Malki, B. Baroux, Influence of cold working on the pitting, *Corros. Sci.* 49 (2007) 1933–1948.
- [51] H.S. Kim, W.J. Kim, Annealing effects on the corrosion resistance of ultrafine-grained pure titanium, *Corros. Sci.* 89 (2014) 331–337.
- [52] I.Y. Nahorna, V.Y. Ol'Shanets'Kyi, Evolution of the dislocation structure of corrosion-resistant steel in the process of plastic deformation, *Mater. Sci.* 40 (2004) 564–567.
- [53] M. Déchamps, F. Baribier, A. Marrouche, Grain boundaries criteria of specialness and deviation from CSL orientation, *Acta Metall.* 35 (1987) 101–107.
- [54] B.W. Reed, M. Kumar, Mathematical methods for analyzing highly-twinned grain boundary networks, *Scr. Mater.* 54 (2006) 1029–1033.
- [55] C. Cayron, Quantification of multiple twinning in face centred cubic materials, *Acta Mater.* 59 (2011) 252–262.
- [56] V.Y. Gertsman, C.H. Henager Jr., Grain boundary junctions in microstructure generated by multiple twinning, *Interface Sci.* 11 (2003) 403–415.
- [57] N. Sakaguchi, Analysis of atomic and electronic structures on CSL boundary in silicon, *J. Jpn. Inst. Met.* 78 (2014) 1–6.
- [58] X.H. Zhu, Y. Xiang, Continuum framework for dislocation structure, energy and dynamics of dislocation arrays and low angle grain boundaries, *J. Mecha. Phys. Solids* 69 (2014) 175–194.
- [59] J.M. Liang, H.B. Wu, D. Tang, P.C. Zhang, X.T. Liu, Influence of inclusion and grain boundary on corrosion behaviour of low alloy steel in cargo oil tank bottom plate environment, *Br. Corros. J.* 49 (2014) 633–642.
- [60] S. Kobayashi, R. Kobayashi, T. Watanabe, Control of grain boundary connectivity based on fractal analysis for improvement of intergranular corrosion resistance in SUS316L austenitic stainless steel, *Acta Mater.* 102 (2016) 397–405.
- [61] C. Hu, S. Xia, H. Li, T.G. Liu, B.X. Zhou, W.J. Chen, N. Wang, Improving the intergranular corrosion resistance of 304 stainless steel by grain boundary network control, *Corros. Sci.* 53 (2011) 1880–1886.
- [62] B. Mantis, N. Sator, B. Guillot, Structure and transport at grain boundaries in polycrystalline olivine: an atomic-scale perspective, *Geochim. Cosmochim. Acta* 219 (2017) 160–176.
- [63] G. Reiss, J. Vancea, H. Hoffmann, Grain boundary resistance in polycrystalline metals, *Phys. Rev. Lett.* 56 (1986) 2100–2103.